Tip-Enhanced Coherent Anti-Stokes Raman Scattering for Vibrational Nanoimaging

Taro Ichimura,[1] Norihiko Hayazawa,[1,4] Mamoru Hashimoto,[2,4] Yasushi Inouye,[3,4,5,*] and Satoshi Kawata[1,4,5]

[1]*Department of Applied Physics, Osaka University, Suita, Osaka 565-0871, Japan*
[2]*Department of Mechanical Engineering and Bioengineering, Osaka University, Toyonaka, Osaka 560-8531, Japan*
[3]*Graduate School of Frontier Biosciences, Osaka University, Suita, Osaka 565-0871, Japan*
[4]*CREST, Japan Corporation of Science and Technology, Japan*
[5]*RIKEN, Wako, Saitama, 351-0198, Japan*

(Received 17 October 2003; published 2 June 2004)

An electric field enhanced by a metallic nanoprobe has locally induced coherent anti-Stokes Raman scattering (CARS) of adenine molecules in a nanometric DNA network structure. Owing to the third-order nonlinearity, the excitation of the CARS polarization is extremely confined to the end of the tip apex, resulting in a spatial resolution far beyond the diffraction limit of light. Our tip-enhanced CARS microscope visualized the DNA network structure at a specific vibrational frequency ($\sim$1337 cm^{-1}) corresponding to the ring-breathing mode of diazole of adenine molecules.

DOI: 10.1103/PhysRevLett.92.220801 PACS numbers: 07.79.Fc, 42.65.Dr, 68.37.Uv

Near-field scanning optical microscopy (NSOM) using an apertureless metallic probe tip has been attracting much attention due to the optical sensing with high spatial resolution beyond the diffraction limit of light. The essential feature of the apertureless NSOM is the use of the electric field enhancement effect at the proximity of the metallic tip end. The field enhancement effect is attributed to the excitation of the local mode of the surface plasmon polaritons (tip plasmon) as well as the singular behavior of the nonretarded field (lightning-rod effect) [1]. At an early stage, it was used to enhance the scattering efficiency of the incident field, giving information similar to a topographic image of the sample structure [2–4]. Since the virtue in optical microscopy is the variety of spectroscopic techniques which can allow for deeper analyses of molecules, many scientists applied the field enhancement effect to the amplification of light emission due to quantum interaction such as fluorescence [5,6], two-photon-excited fluorescence [7], infrared absorption [8,9], and Raman scattering [10–16]. In particular, the tip enhancement of Raman scattering and infrared absorption allow for nanoscale vibrational spectroscopy; hence, they are promising tools that acquire chemical information on molecular species and conformation of nanodevices with nanoscaled spatial resolution.

In order to circumvent the problems of extremely small signals in nanoscaled spectroscopic sensing, in this Letter we propose a combination of a third-order nonlinear optical effect with the field enhancement effect of a metallic tip, that is, a technique for vibrational nanoimaging with tip-enhanced coherent anti-Stokes Raman scattering (CARS), one of third-order coherent nonlinear Raman scatterings [17]. The alternative type of NSOM using an aperture-type probe was previously combined with CARS spectroscopy by Schaller *et al.*, where they employed a fiber probe for the signal collection of CARS excited by an external illumination and demonstrated chemical selective imaging of a biological specimen [18]. The use of tip-enhancement effect is, however, more advantageous with respect to spatial resolution, and is indispensable for observation of a small number of molecules. The excitation of CARS polarization can be further confined spatially and highly enhanced at the very end of the probe tip owing to its third-order nonlinearity, providing higher spatial resolution than tip-enhanced spontaneous Raman scattering. We realized tip-enhanced CARS imaging of a specific vibrational mode of DNA molecules in the fingerprint region with a spatial resolution beyond the diffraction limit of light.

CARS spectroscopy uses three incident fields including a pump field (ω_1), a Stokes field ($\omega_2; \omega_2 < \omega_1$), and a probe field ($\omega_1$), and induces a nonlinear polarization at the frequency of $\omega_{\mathrm{CARS}} = 2\omega_1 - \omega_2$, as shown in Fig. 1(a). When the frequency difference of ω_1 and ω_2 ($\omega_1 - \omega_2$) coincides with one of specific molecular vibrational frequencies (Ω_{Raman}) of Raman-active modes of a given sample, the anti-Stokes Raman signal is resonantly generated. Recently, several scientists have reported that tight focusing of the excitation fields with a high numerical aperture (NA) objective lens can achieve CARS microscopy with three-dimensional imaging capability at a submicron scale [19,20]. The phase matching condition

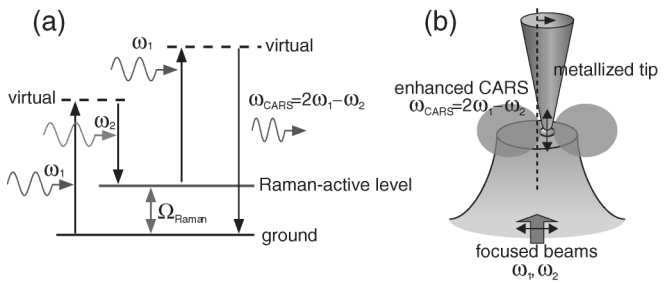

FIG. 1. (a) Energy diagram of coherent anti-Stokes Raman scattering process. (b) Tip enhancement of CARS polarization of molecules near the metallic tip in a tightly focused spot.

can be satisfied automatically in the focused fields of multiple angles [21]. In other words, the phase matching condition is not necessary to consider when the CARS polarizations are generated only in a volume smaller than the propagation wavelength of CARS light [22,23]. In our previous work CARS was strongly amplified by isolated gold nanoparticles, which verified the possibility of the local enhancement of CARS by a metallic nanostructure [24]. Based on the concept mentioned above, one can observe CARS signals generated by the enhanced electric field at a metallic tip end of nanometric scale. Figure 1(b) shows a schematic illustration of CARS generation by a metallic probe tip. Both the incident fields (ω_1 and ω_2) are strongly amplified by the metallic tip in the tightly focused spot and induce CARS polarization with $\omega_{\mathrm{CARS}} = 2\omega_1 - \omega_2$ in the molecules located near the tip. As the z-polarized component of the electric field along the tip axis is dominant in the tip-enhanced field [25], the CARS polarizations are induced along the z direction. For effective coupling of incident fields and tip-enhanced fields, the tip has to be in a position where the incident electric field in the z direction is strong. Since we use linearly polarized beams, the peaks of the z component are found at 200 nm from the center of the focused spot in the direction parallel to the polarization of the incident fields. Thus, the tip is displaced to one of the peaks, as shown in Fig. 1(b). The CARS polarization of molecules is locally generated within the very small volume near the tip so that the ensemble of the induced polarizations behaves as a dipole oscillating in the z direction, as seen in Fig. 1(b). The backscattered component of the radiation can be efficiently collected with the high NA focusing lens. Scanning the sample stage, while keeping the tip at the focused spot, one can acquire two-dimensional tip-enhanced CARS images of a specific vibrational mode with a high spatial resolution that is determined by the size of the tip end rather than the diffraction limited focused spot.

Figure 2 shows the experimental system of the tip-enhanced CARS (TE-CARS) microscopy that we developed. The system mainly consists of two mode-locked Ti:sapphire lasers (pulse duration ~5 ps, spectral band width ~4 cm^{-1}, repetition rate 80 MHz), an inverted optical microscope, and an atomic-force microscope (AFM) using a silicon cantilever tip coated with 20-nm-thick silver film [13–15]. The ω_1 and ω_2 beams are collinearly overlapped in time and space, and introduced into the microscope with an oil-immersion objective lens (NA = 1.4) focused onto the sample surface. The AFM controlled probe tip contacts the sample surface with the constant force and is illuminated by the focused spot. The repetition rate of the excitation lasers is controlled by an electro-optically modulated pulse picker. The backscattered CARS emission is collected with the same objective lens and detected with an avalanche-photodiode (APD) based photon-counting module through an excitation-cut filter and a monochromator (f = 300 mm). The observing spectral width through the detection system is ~12 cm^{-1}. The pulse signals from the APD are counted by a gated photon counter synchronously triggered with the pulse picker. The dark counts are effectively reduced to ~0 counts/s with the gate width of 5 ns. The repetition rate was reduced to 800 kHz to avoid the thermal damage on both the sample and the silver tip while keeping the peak power high.

We used DNA molecules of poly(dA-dT) aggregated into clusters for TE-CARS imaging. The poly(dA-dT) solution in water (250 μg/ml) is cast and dried on a cover slip in the room temperature with the fixation time of ~24 h. The dimensions of the clusters are typically ~20 nm in height and ~100 nm in width. The frequency difference of the two excitation lasers for TE-CARS was set to be 1337 cm^{-1} corresponding to a Raman mode of adenine (ring-breathing mode of diazole) by tuning the excitation frequencies ω_1 and ω_2 to be 12 710 cm^{-1} (λ_1: 786.77 nm) and 11 373 cm^{-1} (λ_2: 879.25 nm), respectively. After the "on-resonant" imaging, the frequency of ω_2 was changed such that the frequency difference corresponds to none of Raman-active vibration ("off-resonant"). Figure 3 shows a spontaneous Stokes Raman spectrum of the DNA in a part of the fingerprint region. The solid arrows on the spectrum denote the

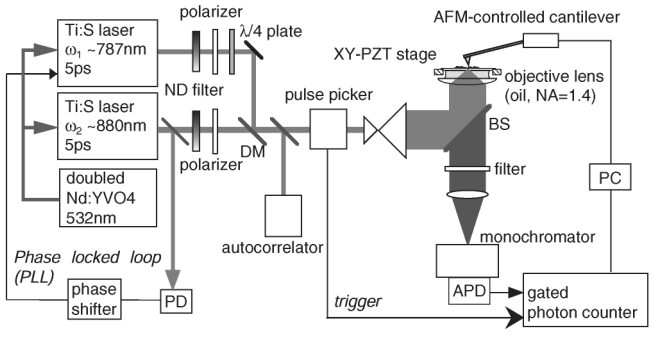

FIG. 2. Schematic of the tip-enhanced CARS microscope.

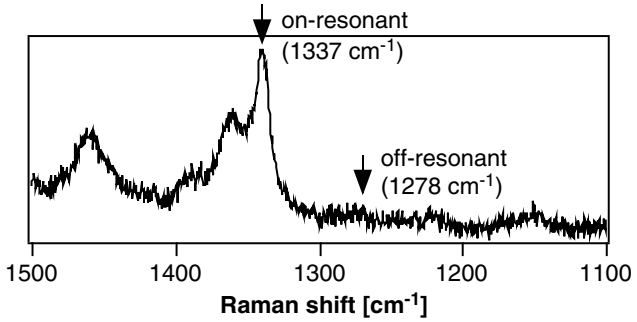

FIG. 3. A spontaneous Raman spectrum of the DNA of poly(dA-dT)-poly(dA-dT). The two frequencies adopted for our TE-CARS imaging are indicated by the downward arrows. The on-resonant frequency at 1337 cm^{-1} can be assigned to the ring-breathing mode of diazole adenine molecule in the DNA.

frequencies adopted for the on-resonant and off-resonant conditions in TE-CARS imaging.

Figure 4 shows the TE-CARS images of the DNA clusters obtained by the TE-CARS microscope. Figures 4(a) and 4(b) are the TE-CARS image at the on-resonant frequency (1337 cm^{-1}) and the simultaneously acquired topographic AFM image. The DNA clusters of ~100 nm diameter are visualized in Fig. 4(a). The two DNA clusters with distance of ~160 nm are obviously distinguished by the TE-CARS imaging. This indicates that the TE-CARS imaging successfully achieved superresolving capability beyond the diffraction limit of light. At the off-resonant frequency (1278 cm^{-1}), the CARS signals mostly vanished in Fig. 4(c). Figures 4(a) and 4(c) verify that vibrationally resonant CARS is emitted from the DNA molecules at the specific frequency. However, there remains some slight signal increase at the clusters at the off-resonant frequency, as seen in Fig. 4(d), which is the same as Fig. 4(c) but is shown with a different grayscale. This can be caused by both the frequency-invariant (nonresonant) component of the nonlinear susceptibility of DNA [17] and the topographic artifact [26]. Figure 4(e) is the far-field CARS image at the on-resonant frequency, which was obtained after removing the tip from the sample. The CARS signal was not detected in the far-field CARS image, which confirms that the CARS polarization is effectively induced by the tip-enhanced field. It can be found that there exists background light in the presence of the tip, as is obvious from Fig. 4(d). This background light is emitted from the silver-coated tip.

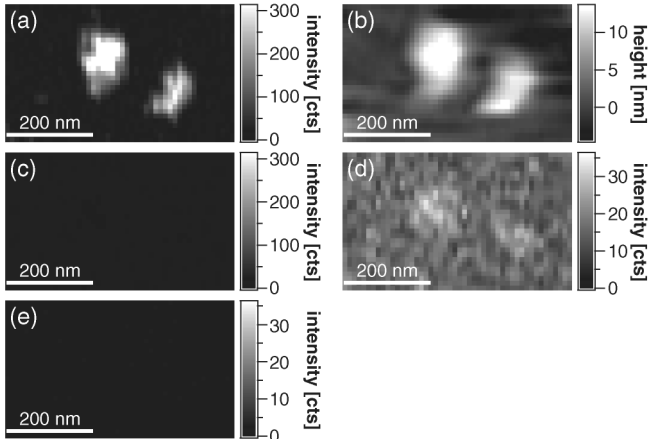

FIG. 4. Tip-enhanced CARS images of the DNA clusters. (a) TE-CARS image at on-resonant frequency (1337 cm^{-1}) and (b) the simultaneously obtained topographic image. (c) TE-CARS image at the off-resonant frequency (1278 cm^{-1}). (d) The same image as (c) shown with a different grayscale. (e) Far-field CARS image of the corresponding area obtained without the silver tip. The scanned area is 500 nm × 300 nm. The number of photons counted in 100 ms was recorded for one pixel. The acquisition time was ~3 min for the image. The average powers of the ω_1 and ω_2 beams were 30 and 15 μW at the 800 kHz repetition rate.

The tip emits light at the same frequency as the CARS ($2\omega_1 - \omega_2$) by the third-order nonlinear susceptibility of silver, which is attributed to local four-wave mixing (FWM). In addition, noble metals such as gold and silver generate white light continuum which is induced by multiphoton excited photoluminescence due to recombination radiation between electrons near Fermi level and photoexcited holes in the d band [27,28]. These two components become background light and compete with the CARS process. In our experiments the dominant background source is the FWM emission as the monochromator was utilized to selectively detect the signal at $2\omega_1 - \omega_2$. The background light can be seen at both the on-resonant and off-resonant frequencies, as they are independent of the molecular vibrations of the sample. Such light emission from a metallic tip degrades the image contrast and signal-to-noise ratio, and subsequently limits the smallest number of molecules that can be observed. In this experiment, however, the tip-enhanced CARS signal intensity largely surpasses the background because the number of molecules in the excited volume is enough to induce the signal.

In order to assess the capability of the sensitivity of the TE-CARS microscopy, we prepared a DNA network of poly(dA-dT)-poly(dA-dT) [29]. DNA [poly(dA-dT)-poly(dA-dT)] dissolved in water (250 μg/ml) was mixed with $MgCl_2$ (0.5 mM) solution, then the DNA solution

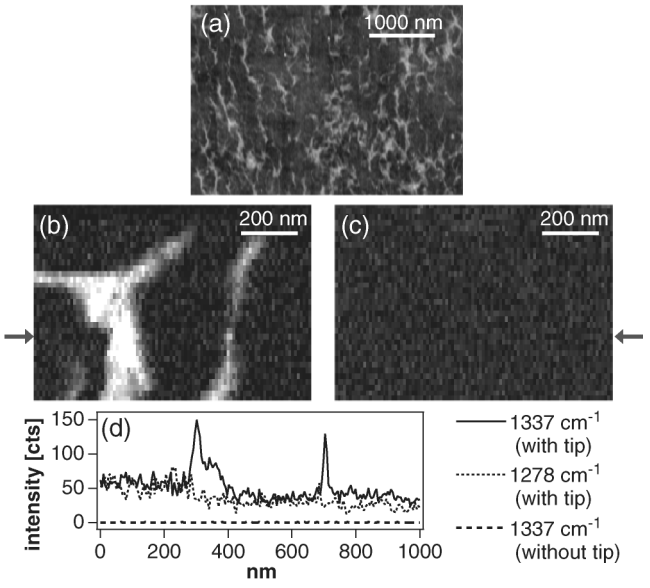

FIG. 5. Tip-enhanced CARS images of the DNA network. (a) Topographic image of the DNA network. (b) TE-CARS image at on-resonant frequency (1337 cm^{-1}). (c) TE-CARS image at the off-resonant frequency (1278 cm^{-1}). (d) Cross sectional line profiles of $y = 270$ nm (indicated by the solid arrows). The scanned area is 1000 nm × 800 nm. The number of photons counted in 100 ms was recorded for one pixel. The acquisition time was ~12 min for the image. The average powers of the ω_1 and ω_2 beams were 45 and 23 μW at the 800 kHz repetition rate.

was cast on a coverslip and blow-dried after the fixation time of ~2 h. Mg^{2+} has a role for the linkage between DNA and oxygen atoms of the glass surface. Figure 5(a) shows a typical topographic image of the DNA network sample. The DNA network consists of bundles of DNA double-helix filaments aligned parallel on the glass substrate. Since the diameter of single DNA double-helix filaments is ~2.5 nm, the height of the bundle structures is ~2.5 nm, and the width is from 2.5 nm (for single filaments) to a few tens of nanometers (for ca. ten filaments). The TE-CARS images at the on- and off-resonant frequencies are shown in Figs. 5(b) and 5(c). The DNA bundles are observed at the resonant frequency in Fig. 5(b), while they cannot be visualized at the off-resonant frequency in Fig. 5(c). This indicates that the observed contrast is dominated by the vibrationally resonant CARS signals. Figure 5(d) shows one-dimensional line profiles at $y = 270$ nm, which were acquired with a ~5 nm step. The line profile of far-field CARS acquired without the silver tip is also added for comparison. Only the TE-CARS in the on-resonant condition has peaks at the positions of $x \sim 370$ nm and $x \sim 700$ nm where adenine molecules exist in the DNA double helix, while the other line profiles do not sense the existence of the molecules. The intensity enhancement factor for each electric field is estimated to be ~100-fold [30,31]. The estimated value of the enhancement factor (~100) is quite realistic and reasonable, as compared to previous numerical results [32,33], although this estimation is very much subject to the changes in each parameter with high-order dependency. We also estimated the size of the locally excited volume of the DNA structure to be ~1 zeptolitre [31]. The smallest detectable volume of DNA under the current experimental condition is estimated as ~1/4 zeptolitre, which is derived from the signal-to-noise ratio of ~15:1 in Fig. 5(d) and the quadratic dependence of the CARS intensity on interaction volume. This indicates that our TE-CARS microscope is capable of sensing a vibrational-spectroscopic signal from an enormously small subzeptolitre volume.

*Corresponding author.
Email address: ya-inoue@ap.eng.osaka-u.ac.jp

[1] *Near-Field Optics and Surface Plasmon Polaritons*, edited by S. Kawata (Springer, Berlin, 2001).
[2] Y. Inouye and S. Kawata, Opt. Lett. **19**, 159 (1994).
[3] P. Gleyzez, A. C. Boccara, and R. Bachelot, Ultramicroscopy **57**, 318 (1995).
[4] L. Novotny, E. J. Sánchez, and X. S. Xie, Ultramicroscopy **71**, 21 (1998).
[5] N. Hayazawa, Y. Inouye, and S. Kawata, J. Microsc. **194**, 472 (1999).
[6] H. F. Hamman, A. Gallagher, and D. J. Nesbitt, Appl. Phys. Lett. **76**, 1953 (2000).
[7] E. J. Sánchez, L. Novotony, and X. S. Xie, Phys. Rev. Lett. **82**, 4014 (1999).
[8] A. Lahrech, R. Bachelot, P. Gleyzes, and A. C. Boccara, Opt. Lett. **21**, 1315 (1996).
[9] B. Knoll and F. Keilmann, Nature (London) **399**, 134 (1999).
[10] Y. Inouye, N. Hayazawa, K. Hayashi, Z. Sekkat, and S. Kawata, Proc. SPIE Int. Soc. Opt. Eng. **3791**, 40 (1999).
[11] R. M. Stöckle, Y. D. Suh, V. Deckert, and R. Zenobi, Chem. Phys. Lett. **318**, 131 (2000).
[12] M. S. Anderson, Appl. Phys. Lett. **76**, 3130 (2000).
[13] N. Hayazawa, Y. Inouye, Z. Sekkat, and S. Kawata, Opt. Commun. **183**, 333 (2000).
[14] N. Hayzawa, Y. Inouye, Z. Sekkat, and S. Kawata, Chem. Phys. Lett. **335**, 369 (2001).
[15] N. Hayazawa, T. Yano, H. Watanabe, Y. Inouye, and S. Kawata, Chem. Phys. Lett. **376**, 174 (2003).
[16] A. Hartschuh, E. J. Sánchez, X. S. Xie, and L. Novotny, Phys. Rev. Lett. **90**, 095503 (2003).
[17] Y. R. Shen, *The Principles of Nonlinear Optics* (Wiley, New York, 1984).
[18] R. D. Schaller, J. Ziegelbauer, L. F. Lee, L. H. Haber, and R. J. Saykally, J. Phys. Chem. B **106**, 8489 (2002).
[19] A. Zumbusch, G. R. Holtom, X. S. Xie, Phys. Rev. Lett. **82**, 4142 (1999).
[20] M. Hashimoto, T. Araki, and S. Kawata, Opt. Lett. **25**, 1768 (2000).
[21] M. Hashimoto and T. Araki, J. Opt. Soc. Am. A **18**, 771 (2001).
[22] J.-X. Cheng, A. Volkmer, and X. S. Xie, J. Opt. Soc. Am. B, **19**, 1363 (2002).
[23] Z. Xiaolin, and R. Kopelman, Ultramicroscopy **61**, 69 (1995).
[24] T. Ichimura, N. Hayazawa, M. Hashimoto, Y. Inouye, and S. Kawata, J. Raman Spectrosc. **34**, 651 (2003).
[25] A. Bouhelier, M. Beversluis, A. Hartschuh, and L. Novotny, Phys. Rev. Lett. **90**, 013903 (2003).
[26] B. Hecht, H. Bielefeldt, Y. Inouye, D.W. Pohl, and L. Novotny, J. Appl. Phys. **81**, 2492 (1997).
[27] G. T. Boyd, Z. H. Yu, and Y. R. Shen, Phys. Rev. B **33**, 7923 (1986).
[28] J. P. Wilcoxon and J. E. Martin, J. Chem. Phys. **108**, 9137 (1998).
[29] S. Tanaka, L. T. Cai, H. Tabata, and T. Kawai, Jpn. J. Appl. Phys. **40**, L407 (2001).
[30] For the estimation of the enhancement factor we preliminarily measured far-field CARS intensity of a DNA cluster with different excitation power and repetition rate, then estimated the efficiency of the CARS emission per unit volume, peak power, and repetition rate. Using the estimated efficiency, the enhancement factor was derived.
[31] For the estimation of the excited volume we assume the tip-enhanced local excitation spot to be a sphere with 20 nm diameter centered at the tip end in which the excitation efficiency is uniform. The locally excited volume is defined as the volume overlapped by the excitation spot and the sample. In these assumptions, the excited volume is approximately a column with 2.5 nm height and 20 nm diameter.
[32] H. Furukawa and S. Kawata, Opt. Commun. **148**, 221 (1998).
[33] J. T. Krug II, E. J. Sánchez, and X. S. Xie, J. Chem. Phys. **116**, 10 895 (2002).